

# Synthesis, characterization and bioactivity studies of novel 1,3,4-oxadiazole small molecule that targets basic phospholipase A<sub>2</sub> from *Vipera russelli*

Vivek Hamse Kameshwar<sup>1</sup> · Kumar J. R.<sup>2</sup> · Babu S. Priya<sup>3</sup> · S. Nanjunda Swamy<sup>1</sup>

Received: 4 July 2016 / Accepted: 15 November 2016  
© Springer Science+Business Media New York 2016

**Abstract** Secretory phospholipase A<sub>2</sub> (sPLA<sub>2</sub>) is a key enzyme participating in the inflammatory cascade followed by the action of cyclooxygenase-2 and lipoxygenases. Therefore, inhibitors of sPLA<sub>2</sub> could be used as potent anti-inflammatory agents to treat the early phase of inflammation. In this study, we have prepared the fenoprofen and ibuprofen analogs containing 1,3,4-oxadiazole nucleus and tested against *Vipera russelli* venom's basic sPLA<sub>2</sub> (VRV-PL-VIIIa). Among the tested ligands **5(a-t)**, 2-(2-chlorophenyl)-5-(1-(4-phenoxyphenyl) ethyl)-1,3,4-oxadiazole (**5m**) inhibited the catalytic activity of VRV-PL-VIIIa with an IC<sub>50</sub> value of 11.52 μM. Biophysical studies revealed that the **5m** quenches the intrinsic fluorescence of VRV-PL-VIIIa, in a concentration dependent manner. Also, the compound **5m** affected VRV-PL-VIIIa conformation, which was observed by circular dichroism spectra that recorded the prominent shift in the α-helix peak and the random coil formation of VRV-PL-VIIIa. Further, molecular docking analysis revealed that the compound **5m** possess strong hydrophobic interactions at catalytic triad region of the VRV-PL-VIIIa. Evident to in vitro and in silico studies, **5m** strongly inhibited the hemolysis of red

blood cells. Our in vivo pharmacological studies revealed that the compound **5m** inhibited the edematogenic activity of VRV-PL-VIIIa in mouse foot pad. Additionally, the **5m** inhibited VRV-PL-VIIIa-induced myotoxicity and lung hemorrhage in mice. Overall, our ADMET results depicted that **5m** possess better druggable property. Thus, this study explored the new fenoprofen and ibuprofen analog **5m** as the lead-structure that serves as an anti-inflammatory agent.

**Keywords** 1,3,4-Oxadiazole · VRV-PL-VIIIa · Anti-inflammation · NSAIDs · ANS

## Introduction

Venom of venomous snakes acts as natural advance killer machines to kill its prey, among which *V. russelli* is one of the most dangerous species found in the Indian subcontinent and other parts of Asia, causing high morbidity and mortality rate among the big four venomous snakes [1]. Annual snakebite is a majorly neglected medical emergency reported in modern India representing about 45,900 annual deaths affecting to a very great degree in rural areas (97%). It is found in order as Uttar Pradesh > Andhra Pradesh > Bihar. Sex ratio of the victim bitten by snake were more common in males (59%) than females (41%) which contributing 25% at ages of 15–29 years during the monsoon months of June–September. Hence, an effective treatment involving both education and antivenom provision would reduce snakebite deaths globally [2].

Among the big four family, Viperidae family snake venom possess sPLA<sub>2</sub> enzyme belonging to group II, whose enzymatic activity is critical with the presence of amino acid residue of His48 and Asp49 (VRV-PL-VIIIa-venom of *Russelli viper* phospholipase A<sub>2</sub> VIIIa peak).

**Electronic supplementary material** The online version of this article (doi:10.1007/s11010-016-2888-6) contains supplementary material, which is available to authorized users.

✉ S. Nanjunda Swamy  
nanju\_chem@yahoo.com; nanjuchem@gmail.com

<sup>1</sup> Department of Biotechnology, JSS Science and Technology University, Mysuru 570006, India

<sup>2</sup> Department of Biochemistry, Faculty of Life Sciences, JSS University, Mysuru, India

<sup>3</sup> Department of Studies in Chemistry, University of Mysore, Manasagangotri, Mysuru 570006, India

Since Gly30 and Asp49 are among the highly conserved residues in PLA<sub>2</sub> enzymes residing at catalytic triad. Carbonyl group of Asp49 forms a hydrogen bond with the Ca<sup>2+</sup> ion which is very crucial for the Ca<sup>2+</sup> ion to interact with the substrate for catalysis [3, 4]. The pathophysiology of basic VRV-PL-VIIIa is that, it exerts its local intense toxicity effects and systemic effects [5]. sPLA<sub>2</sub> is a primary upstream enzyme, which cleaves fatty acids at the *sn*-2 position of glycerol, the backbone of phospholipids releasing free fatty acid and lysophospholipid [6, 7], which are substrates for downstream enzymes like cyclooxygenase (COX-2), lipoxygenase (LOXs), and lysophospholipid acyl-CoA acyltransferase (LAT). The reaction has particular importance when the fatty acid released from the *sn*-2 position is arachidonic acid, which is further oxidatively metabolized by downstream enzymes like COX-2 and LOX enzymes, resulting in the release of proinflammatory mediators like prostaglandins, thromboxanes, and leukotrienes [8–10]. Specific inhibitor which can block sPLA<sub>2</sub> could have significant anti-inflammatory property, which blocks the substrate for COX-2 and LOXs.

Currently, Nonsteroidal anti-inflammatory drugs (NSAIDs) are used to treat acute as well as chronic inflammatory conditions targeting COX-2. Continuous use of NSAIDs results in an unacceptable risk like Gastrointestinal-adverse drug reactions (GI-ADRs), associated with the renal and cardiovascular system failure, due to the presence of a free carboxylic acid group of NSAIDs (fenopfen and ibuprofen) [11]. Previously, findings suggested that cyclization of the free carboxylic group of aroyl propionic acid resulted in significant decrease of ulcerogenic activity [12]. The presence of bulky ester group in these ligands was responsible for the inhibition of venom PLA<sub>2</sub>. In medicinal chemistry, the 1,3,4-oxadiazole-based heterocyclic ring was used as replacements for ester bonds [13]. Also, oxadiazole, a 5-membered heterocyclic ring, was used for designing potent bioactive entities [13, 14]; Henceforth, we focused to prepare anti-inflammatory drugs like fenopfen and ibuprofen analogs, which contain 1,3,4-oxadiazole ring by replacing the terminal-free carboxylic group to target sPLA<sub>2</sub> of *V. russelli*. Further, this is the first study to report the anti-PLA<sub>2</sub> activity of the newly synthesized ligands containing 1,3,4-oxadiazole elucidating better correlation between CD data and Kabsch–Sander's secondary structural prediction along with in silico studies validating our findings.

## Materials and methods

Lyophilized powder of *V. russelli* venom was purchased from Iruela Co-operative Society Ltd., Chennai, India. Fenopfen calcium, ibuprofen, 2-methylbenzoic acid, 2,3-dimethylbenzoic acid, 4-methylbenzoic acid, 2,5-dimethylbenzoic acid,

2-chlorobenzoic acid, 2,3-dichlorobenzoic acid, 8-anilino-1-naphthalenesulfonic acid (ANS), 1,2-dimyristoyl-*sn*-glycero-3-phosphocholine (DMPC), Sephadex G-75, Sephadex G-50, and CM-Sephadex C-25 were purchased from Sigma–Aldrich, India. 1-myristoyl-2-hydroxy-*sn*-glycero-3-phosphocholine (LPC) was purchased from Avanti Polar Lipids. HPLC grade Methanol and analytical grade HCl were obtained from Fisher Scientific. Tris (hydroxymethyl) aminomethane, fatty acid-free bovine serum albumin (BSA) fraction V, Sodium hydroxide, Silica gel (60–120 mesh), DMSO, pre-coated TLC plates, Acetonitrile, Ethyl acetate, Calcium chloride dihydrate, and Sodium chloride were purchased from Merck. Triton X-100 was obtained from HiMedia Laboratories. Sodium acetate, glycine, and ethylene glycol bis (β-aminoethyl ether) N, N<sup>1</sup>-tetraacetic acid (EGTA) were purchased from SRL Chemicals. Milli-Q water was used throughout the experiments. All chemicals were of analytical grade, and solvents were of HPLC grade. Nanodrop ND3300 Fluorospectrometer from Thermo Scientific was used to record the fluorescence. This study was carried out in accordance with Animal ethical committee of the JSS Medical College, Mysuru, India. The protocol was approved by the Institutional Animal Ethics Committee (IAEC) on the Ethics of Animal Experiments. (Registration no 261/CPSCE, dated October 16 Oct, 2000; Sanctioned letter no JSSMC/PR/IAEC/24/2091/2013-14, dated July 29, 2013). Healthy Swiss albino male mice weighing 20–25 g were obtained from Central animal house facility, JSS Medical College, Mysuru. All dissection was performed under sodium pentobarbital anesthesia, followed by euthanasia (cervical dislocation) to minimize suffering.

## General procedure for the synthesis of 2,5 disubstituted 1,3,4-oxadiazole derivatives 5(a–t)

Aromatic acids **1(a–d)** were refluxed for 3–4 h with 6.5 ml of ethanol containing 5–6 drops of concentrated H<sub>2</sub>SO<sub>4</sub>. Progress of reaction was monitored and confirmed by TLC (hexane:ethyl acetate:7:3), the reaction mass was extracted with dichloromethane thrice. The solvent was evaporated under vacuum, to obtain aryl benzoates. Resultant aryl benzoates **2(a–d)** were added dropwise to 6–8 ml of ethanol containing 100% NH<sub>2</sub>NH<sub>2</sub>.H<sub>2</sub>O (6.5 ml), and the reaction mass was refluxed for 8–10 h. The solvent was evaporated under vacuum completely. Resultant residual mass was stirred with 5–6 ml of water at 5–8 °C and filtered. The pure crystalline compounds were obtained by recrystallizing it in ethyl acetate to yield aryl hydrazides **3(a–d)**. The reaction mixture containing aryl hydrazides **3(a–d)** (0.002 mol) and aromatic acids **4(a–f)** (0.001 mol) were dissolved in 8 ml of phosphorous oxychloride and refluxed for 4–6 h under nitrogen. The reaction mixture was cooled to room temperature and quenched using

crushed ice. On neutralization of the contents, resultant mass was washed with 20% sodium bicarbonate solution followed by brine wash. Resultant residual product was dried, and recrystallization was done using ethyl acetate to give **5(a–t)** as shown in Table 1. Spectral properties were consistent with their assigned structures.

### Purification of sPLA<sub>2</sub> (VRV-PL-VIIIa) from *V. russelli* venom

sPLA<sub>2</sub> from *V. russelli* venom was purified to homogeneity as reported earlier [5]. Protein was estimated by Lowry's method [15]. Briefly, *V. russelli* venom (100 mg) was fractionated on pre-equilibrated Sephadex G-75 column (1.5 × 140 cm) using 50 mM phosphate buffer pH 7.0. The protein was resolved into major three peaks. The second peak, constituting about 30% of the total protein, showed major sPLA<sub>2</sub> activity. This sPLA<sub>2</sub> peak fraction was lyophilized and further subjected to pre-equilibrated CM-Sephadex C-25 column (1.5 × 40 cm) chromatography. The fractions were eluted stepwise using phosphate buffers of varied ionic strength (50–200 mM) and pH (7.0–8.0). They were resolved into two fractions labeled as V and VIII, respectively. The above eluted two fractions were similar to V and VIII protein profiles as reported earlier [5]. The lyophilized fraction VIII was next subjected to Sephadex G-50 column (1.0 × 40 cm) chromatography and eluted using 50 mM phosphate buffer pH 7.0, and the obtained peak was checked for sPLA<sub>2</sub> activity. Homogeneity was checked by SDS-PAGE and RP-HPLC as reported earlier [5] (data not shown).

### In vitro inhibition of VRV-PL-VIIIa by 2,5 disubstituted 1,3,4-oxadiazole derivatives **5(a–t)**

sPLA<sub>2</sub> activity was assayed according to the reported method [16]. Briefly, a 50 µl buffer containing 50 mM Tris–HCl buffer pH 7.5, 10 mM CaCl<sub>2</sub>, and 100 µM

substrate stock (1 mM DMPC in methanol containing 2 mM Triton X-100 in Milli-Q water) was added and incubated for 5 min at 37 °C. Activity was initiated by adding 10 ng of sPLA<sub>2</sub> alone or pre-incubated with different concentrations of **5(a–t)** ranging from 0 to 100 µM for 5 min at 37 °C. Reaction mixtures were incubated for 45 min at 37 °C. 50 µl of quenching solution was added at a final concentration of 2 mM NaN<sub>3</sub>, 50 µM ANS, and 50 mM EGTA, vortexed for 30 s, and incubated for 5 min at RT. 2 µl of this solution was pipetted to measure RFU in a Nanodrop ND3300 Ver 2.8 using an excitation UV-LED (370 ± 10 nm) and emission was recorded at 480 nm in dark condition. Enzyme activity was calculated by Eq. (A.1), where ΔRFU is the change in RFU of test (with sPLA<sub>2</sub>) with respect to control (without sPLA<sub>2</sub>) in the presence of inhibitor(s). The resultant RFU was compared with the standard LPC curve to determine the sPLA<sub>2</sub> activity in the presence of inhibitor [16].

### Intrinsic fluorescence spectra of sPLA<sub>2</sub>-5m adduct

Quenching studies of deeply buried aromatic amino acid residues at active site were performed in the presence of sPLA<sub>2</sub> with and without inhibitor (**5m**) after excitation at 280 nm. 1 ml of reaction mixture containing 30 µg of sPLA<sub>2</sub>, 10 mM CaCl<sub>2</sub>, 20 mM Tris–HCl buffer, pH 7.5, with different concentrations of inhibitor **5m** (0–100 µM) was incubated at 37 °C for 10 min. Fluorescence emission spectra (395–500 nm) of sPLA<sub>2</sub> alone and mixture of sPLA<sub>2</sub>-**5m** were recorded. Tryptophan was used as standard to correct non-specific quenching of enzyme with an inhibitor.

### Circular dichroism studies

Binding study of **5m** with sPLA<sub>2</sub> was carried out by UV-CD spectrum in the absence and presence of **5m** at 5 µM concentration, using Jasco J715 spectropolarimeter.

**Table 1** List of 2,5 disubstituted 1, 3, 4-oxadiazole derivatives **5(a–t)**

Ligands	R	R <sub>1</sub>	Ligands	R	R <sub>1</sub>
<b>5a</b>	2-Cl C <sub>6</sub> H <sub>5</sub>	4-Cl C <sub>6</sub> H <sub>5</sub> ( <b>4a</b> )	<b>5k</b>	2-CH <sub>3</sub> C <sub>6</sub> H <sub>5</sub>	2,3-CH <sub>3</sub> C <sub>6</sub> H <sub>5</sub> ( <b>4d</b> )
<b>5b</b>	2,3-Cl <sub>2</sub> C <sub>6</sub> H <sub>4</sub>	4-Cl C <sub>6</sub> H <sub>5</sub> ( <b>4a</b> )	<b>5l</b>	2,3-CH <sub>3</sub> C <sub>6</sub> H <sub>5</sub>	2,3-CH <sub>3</sub> C <sub>6</sub> H <sub>5</sub> ( <b>4d</b> )
<b>5c</b>	2-CH <sub>3</sub> C <sub>6</sub> H <sub>5</sub>	4-Cl C <sub>6</sub> H <sub>5</sub> ( <b>4a</b> )	<b>5m</b>	2-Cl C <sub>6</sub> H <sub>5</sub>	Fenoprofen ( <b>4e</b> )
<b>5d</b>	2,3-CH <sub>3</sub> C <sub>6</sub> H <sub>4</sub>	4-Cl C <sub>6</sub> H <sub>5</sub> ( <b>4a</b> )	<b>5n</b>	2,3- Cl <sub>2</sub> C <sub>6</sub> H <sub>4</sub>	Fenoprofen ( <b>4e</b> )
<b>5e</b>	2-Cl C <sub>6</sub> H <sub>5</sub>	2,5-CH <sub>3</sub> C <sub>6</sub> H <sub>4</sub> ( <b>4b</b> )	<b>5o</b>	2-CH <sub>3</sub> C <sub>6</sub> H <sub>5</sub>	Fenoprofen ( <b>4e</b> )
<b>5f</b>	2,3-Cl <sub>2</sub> C <sub>6</sub> H <sub>4</sub>	2,5-CH <sub>3</sub> C <sub>6</sub> H <sub>4</sub> ( <b>4b</b> )	<b>5p</b>	2,3-CH <sub>3</sub> C <sub>6</sub> H <sub>4</sub>	Fenoprofen ( <b>4e</b> )
<b>5g</b>	2-CH <sub>3</sub> C <sub>6</sub> H <sub>5</sub>	2,5-CH <sub>3</sub> C <sub>6</sub> H <sub>4</sub> ( <b>4b</b> )	<b>5q</b>	2-Cl C <sub>6</sub> H <sub>5</sub>	Ibuprofen ( <b>4f</b> )
<b>5h</b>	2,3-CH <sub>3</sub> C <sub>6</sub> H <sub>4</sub>	2,5-CH <sub>3</sub> C <sub>6</sub> H <sub>4</sub> ( <b>4b</b> )	<b>5r</b>	2,3- Cl <sub>2</sub> C <sub>6</sub> H <sub>4</sub>	Ibuprofen ( <b>4f</b> )
<b>5i</b>	2-CH <sub>3</sub> C <sub>6</sub> H <sub>5</sub>	2-CH <sub>3</sub> C <sub>6</sub> H <sub>5</sub> ( <b>4c</b> )	<b>5s</b>	2-CH <sub>3</sub> C <sub>6</sub> H <sub>5</sub>	Ibuprofen ( <b>4f</b> )
<b>5j</b>	2,3-CH <sub>3</sub> C <sub>6</sub> H <sub>4</sub>	2-CH <sub>3</sub> C <sub>6</sub> H <sub>5</sub> ( <b>4c</b> )	<b>5t</b>	2,3-CH <sub>3</sub> C <sub>6</sub> H <sub>4</sub>	Ibuprofen ( <b>4f</b> )

Briefly, 1 ml reaction mixture containing 0.2 mg/ml concentration of sPLA<sub>2</sub>, 10 mM Tris–HCl buffer pH 7.5, 10 mM CaCl<sub>2</sub>, and with/without **5m** was added and the spectrum was recorded at RT between 195 and 260 nm using quartz cuvette with path length of 1 cm. The bandwidth and response time were 2 nm and 2 s, respectively. The protein spectrum was corrected by subtracting a blank solution containing 10 mM Tris–HCl buffer (pH 7.5) and 10 mM CaCl<sub>2</sub>. The scale on the CD spectra was normalized to mean residue ellipticity (MRE), which was measured in degrees cm<sup>2</sup> d mol<sup>-1</sup> residue using Eq. (B.1), where  $\Theta$  is raw ellipticity measured in machine units (millidegrees). The mean residue weight (MRW) for the peptide bond was calculated from Eq. (B.2), where  $M$  is the molecular mass of the polypeptide chain (in Da);  $N$  is the number of amino acids present in the target protein;  $l$  is the path length in cm; and  $[P]$  is the protein concentration in mg/ml [17]. The MRE was plotted against the corresponding wavelength. Secondary structure calculations of CD spectra were determined by using K2D3 server [18].

### Inhibitor-binding analysis using ANS as fluorescence probe

The 50  $\mu$ l reaction mixture containing 100  $\mu$ M substrate and different concentrations of inhibitor **5m** (0–100  $\mu$ M) in 50 mM Tris–HCl buffer, pH 7.4, and 10 mM CaCl<sub>2</sub> was incubated for 10 min at 37 °C. Fifty microliters of quenching solution was prepared and added as mentioned earlier and vortexed for 30 s and incubated for 5 min at RT. Two microliters of this solution was pipetted to measure RFU. Emission coefficient (EC) was measured as the slope of the plot of fluorescence intensity as a function of ANS along with DMPC complex in the presence or absence of **5m**:  $EC = Em_t/Em_b$ , where  $Em_t$  and  $Em_b$  are the ECs of ANS in the ternary (DMPC-**5m**-ANS) and in the binary (DMPC-ANS) complexes, respectively.

### In silico molecular docking studies

The structural drawing and geometry cleaning of the 2,5 disubstituted 1,3,4-oxadiazole derivatives **5(a–t)** were performed in Maestro 9.3 and then subjected to other parameters, namely, energy minimization by using OPLS 2005 force field. The crystal structure of a VRV-PL-VIIIa from *V. russelli*, complex with 2-hydroxy-4-aminobenzoic acid (PDB ID: 1SXX, 1.2 Å resolution) [19], was retrieved through Brookhaven protein data bank (PDB). Crystal structure was imported and refined by a multistep process through the protein preparation wizard of Maestro 9.3, which includes energy minimization using OPLS-2005

force field. Using PROPKA, pH was fixed and optimized to 7.5. Non-hydrogen atoms were minimized by restrained minimization to default RMSD to 0.3 Å. The docking study of selected target and ligands **5(a–t)** was done by using Maestro 9.3, docking module Glide XP (extra precision). Receptor grid generation of VRV-PL-VIIIa was defined as Asp47, His48, and Gly30 to prepare a grid box of 30 Å x 30 Å x 30 Å size to dock ligands. Docking precision and ligand sampling were fixed to flexible mode. Twenty numbers of poses per ligands were chosen for accurate docking with the target. The resultant output file was visualized on maestro; further, the docking calculation was analyzed and validated by comparing with the standard inhibitor. Additionally, molecular dynamics (MD) simulations were performed after the docking simulations to confirm the stability of the ligand in the proposed site with the Desmond program inbuilt OPLS 2005. VRV-PL-VIIIa-**5m** complex was positioned in an orthorhombic cell soaked with a pre-equilibrated box of explicit solvent including 10 mM CaCl<sub>2</sub> salt with single-point charge (SPC) water model in a cubic box with 10 Å x 10 Å x 10 Å dimension. Overlapping solvent molecules were removed, and an appropriate number of counter ions were added to maintain charge neutrality and energy minimization for both SPC water models and the protein before subjecting the system to MD simulation runs [20].

### Inhibition of indirect hemolytic activity by 2,5 disubstituted 1,3,4-oxadiazole derivatives

Indirect hemolytic activity was assayed according to the method of Boman and Kalletta [21]. Briefly, packed human erythrocytes, egg yolk, and phosphate-buffered saline pH 7.5 were mixed in the ratio of 1:1:8 (v/v). 1 ml of this suspension was incubated separately for 60 min at 37 °C with 8  $\mu$ g of sPLA<sub>2</sub> alone or pre-incubated with different concentrations of inhibitor **5m** ranging from 0 to 100  $\mu$ M for 5 min at RT. Reaction was stopped by adding 9 ml of ice-cold PBS with pH 7.5; reaction mixtures were centrifuged at 4 °C for 10 min at 1500 $\times$ g. The resultant % of hemoglobin released in supernatant was measured spectrophotometrically at 540 nm.

### Neutralization of edema-inducing activity of sPLA<sub>2</sub>

The procedure of Yamakawa et al. [22], as modified by Vishwanath et al., on groups of four animals each [23] was followed. Swiss albino male mice weighing 20–25 g were injected with 8  $\mu$ g of sPLA<sub>2</sub> (VRV-PL-VIIIa) with and without **5m** (0–200  $\mu$ M) in a total volume of 30  $\mu$ l saline

into the intraplantar surface of the right hind footpad. Left footpad received 30  $\mu\text{l}$  of saline and served as vehicle. After 45 min, the mice were sacrificed by giving anesthesia (pentobarbitone, 30 mg/kg) through i.p, and both hind limbs were removed at the ankle joint and weighed individually after cervical dislocation. The increase in weight due to edema is expressed as Eq. (C.1) Percentage increase of sham-injected control compared to the un-injected limb was found to be  $175 \pm 4\%$ .

### Myotoxicity

Myotoxicity was determined as reported earlier in groups of four animals each [24]. Briefly, half the LD<sub>50</sub> value [5] (5.3 mg/kg body weight) of VRV-PL-VIIIa in 100  $\mu\text{l}$  saline was injected intramuscularly into the right thigh of positive control grouped mice ( $n = 4$ ). The groups are receiving 100  $\mu\text{l}$  saline (vehicle) or only **5m** in saline served as negative control. For inhibition studies, the sPLA<sub>2</sub> was pre-incubated with the inhibitor in the ratio of 1:5 (sPLA<sub>2</sub>:**5m**, w/w) for 15 min before injecting intramuscularly (test). After 4 h of administration of respective controls and test samples, mice were anesthetized by administering pentobarbitone (30 mg/kg, i.p) and sacrificed by cervical dislocation. The abdominal cavity was opened, and blood was drawn by puncturing the aorta. The 1:20 diluted serum was estimated for cytosolic markers like AST, LDH, and CK levels by Agappe diagnostic kits using Toshiba TBA 40FR Accute analyzer. Activities were expressed as units/l.

The thigh muscle tissue was dissected from the site of injection and fixed in Bouin's solution followed by sequential dehydration by processing the tissue through different grades of alcohol and chloroform:alcohol mixture. The processed tissue was embedded in paraffin block and cut into 3  $\mu\text{M}$ –4  $\mu\text{M}$  thin sections. The sections were stained with hematoxylin and eosin for microscopic observation. The sections were observed under a microscope, and photographs were taken using Jenoptik camera (ProgResCapturePro<sup>®</sup>) attached to the microscope.

### Lung hemorrhage

Lung hemorrhage was determined as reported earlier in groups of four animals each [24]. Half the LD<sub>50</sub> value of VRV-PL-VIIIa in 100  $\mu\text{l}$  saline was injected intraperitoneally (i.p) into the positive control grouped mice ( $n = 4$ ). The groups received 100  $\mu\text{l}$  saline (vehicle) or only inhibitor **5m** in saline served as negative control. For inhibition studies, the sPLA<sub>2</sub> was pre-incubated with the inhibitor in the ratio of 1:5 (sPLA<sub>2</sub>:**5m**, w/w) for 15 min

before injecting intraperitoneally(test). After 4 h of administration of respective controls and test samples, mice were anesthetized by administering pentobarbitone (30 mg/kg, i.p) and sacrificed by cervical dislocation. The lung tissue was dissected, processed, and visualized as mentioned above.

### Statistical analysis

Results were presented as the mean  $\pm$  SEM. Two-way ANOVA followed by Dunnett's multiple comparisons test and Sigmoidal four parametric logical (4PL) fit was computed and analyzed using the GraphPad Prism<sup>®</sup>V.6.05 (GraphPad Software, Inc., USA). Statistical significance was represented as \* $P < 0.05$ , \*\*\* $P < 0.001$ , \*\*\*\* $P < 0.0001$ .

## Results

### Chemical synthesis of 1,3,4-oxadiazoles

The title compounds were synthesized by reacting aryl hydrazides **3(a–d)** with various aromatic acids **4(a–f)** (0.001 mol) in the presence of the cyclizing agent phosphorous oxychloride by refluxing the mixture under nitrogen atmosphere (Scheme 1). The resultant residual product was dried and recrystallized using ethyl acetate to obtain title compounds **5(a–t)** (Table 1). Spectral properties were consistent with their assigned structures.

### In vitro inhibitory effect of 1,3,4-oxadiazoles on VRV-PL-VIIIa

The 1,3,4-oxadiazole ring underwent nucleophilic attack at carbon, followed by ring cleavage and electrophilic attack at nitrogen [25]. The series of 1,3,4-oxadiazoles **5(a–t)** were assessed for PLA<sub>2</sub> inhibition studies, and the results are tabulated in Table 2. The tested 2,5-disubstituted-1,3,4-oxadiazoles **5(a–t)** inhibited sPLA<sub>2</sub> in dose-dependent manner with an IC<sub>50</sub> value ranging from 11.52 to 72  $\mu\text{M}$  which are computed and analyzed using sigmoidal 4PL curve fit. Among the tested compounds, **5m** showed significant inhibition against VRV-PL-VIIIa with IC<sub>50</sub> value of 11.52  $\mu\text{M}$  (Fig. 1), when compared to other structurally related molecules. Overall the result indicates that dimethyl/mono chloro at ortho position in *R* is most favorable for inhibition of VRV-PL-VIIIa in terms of hydrophobicity (**5j**) and electronegative (**5e**), respectively (Table 2). With this view, we derivatized fenoprofen with 1,3,4 oxadiazole nucleus where mono chloro/dimethyl group was present at ortho position in case *R* of **5m** to **5p**.

**Scheme 1** Substituted aromatic acids **1(a-d)** are converted into the corresponding esters **2(a-d)**. These esters were converted into the corresponding hydrazides **3(a-d)**. Aryl hydrazides **3(a-d)** cyclized with aromatic acids from **4(a-f)** were coupled in the presence of phosphorous oxychloride under reflux, to give respective 2,5-disubstituted 1, 3, 4-oxadiazoles derivatives **5(a-t)** as mentioned in Table 1

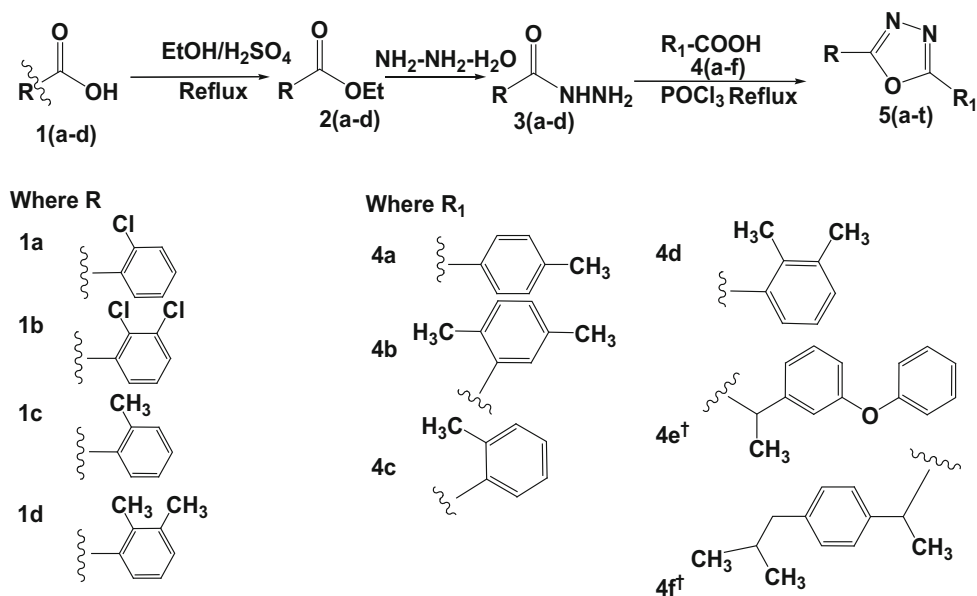


**Table 2** In vitro and in silico anti-inflammatory activity of 2,5 disubstituted 1, 3, 4-oxadiazole derivatives (Scheme 1)

Ligands	In vitro assay 4PL fit IC <sub>50</sub> (μM)	In silico analysis			
		Glide Emodel (kcal/mol)	XP G-score	Glide energy (kcal/mol)	Glide ligand efficiency
<b>5a</b>	41.58	-29.44	-3.41	-22.34	-0.81
<b>5b</b>	44.41	-36.98	-3.38	-26.01	-0.78
<b>5c</b>	49.68	-28.10	-3.07	-21.22	-0.74
<b>5d</b>	29.45	-37.99	-3.87	-22.74	-0.89
<b>5e</b>	27.22	-33.16	-3.89	-20.33	-0.90
<b>5f</b>	61.12	-34.15	-0.15	-30.05	-0.04
<b>5g</b>	52.26	-35.40	-2.90	-27.26	-0.72
<b>5h</b>	72.18	-33.79	3.15	-27.67	0.79
<b>5i</b>	31.40	-37.53	-3.83	-24.15	-0.88
<b>5j</b>	23.75	-44.01	-4.21	-34.71	-0.98
<b>5k</b>	60.18	-36.96	-2.64	-27.76	-0.66
<b>5l</b>	70.14	-30.88	1.89	-25.55	0.47
<b>5m</b>	11.52	-44.87	-6.40	-34.80	-1.03
<b>5n</b>	35.04	-33.58	-3.47	-25.57	-0.87
<b>5o</b>	30.45	-32.44	-3.85	-24.56	-0.90
<b>5p</b>	57.92	-30.61	-2.86	-23.71	-0.72
<b>5q</b>	41.33	-43.74	-3.46	-30.59	-0.80
<b>5r</b>	32.78	-33.06	-3.62	-25.95	-0.84
<b>5s</b>	32.70	-36.71	-3.63	-23.07	-0.84
<b>5t</b>	25.84	-35.60	-4.09	-20.06	-0.95
Quercetin	2.0	-40.54	-1.86	-32.20	-0.46

### Intrinsic fluorescence spectra of sPLA<sub>2</sub>-5m adduct

Intrinsic fluorescence of purified VRV-PL-VIIIa (sPLA<sub>2</sub>) with lead molecule **5m** alone gives the maximum intensity corresponding to tryptophan amino acid [26] as showed in

Fig. 2a. Addition of **5m** quenched the intrinsic fluorescence spectra of sPLA<sub>2</sub> enzyme in a dose-dependent manner. The RFU of VRV-PL-VIIIa decreases as the inhibitor concentration increased (Fig. 2b).

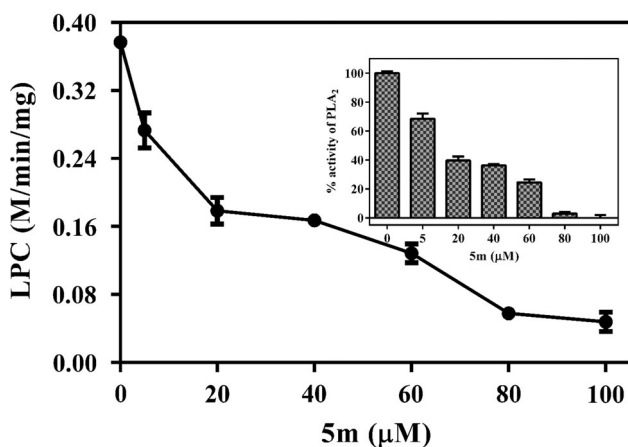


**Fig. 1** Dose response curves showing the effect of **5m** on VRV-PL-VIIIa.  $IC_{50}$  was calculated using sigmoidal four parameter logistic fit (4PL) plot. *Inset* percentage of sPLA<sub>2</sub> activity in the presence of **5m** (0–100 μM). All data values represent mean  $\pm$  SEM ( $n = 6$ )

### Circular dichroism studies

Far UV-CD spectra of VRV-PL-VIIIa enzyme with/without **5m** were evaluated for major characteristic changes initiated between 195 and 222 nm. In the presence of 5 μM concentration of **5m** ( $\approx$  half  $IC_{50}$  value) [26], it was found that enzyme peak deviate steeply downward compared to the native structure. From 208 nm to 202 nm a large steep negative peak was observed confirming the quenching of  $\alpha$ -helix in the presence of **5m** wherein active site amino acid of VRV-PL-VIIIa resides from 39 to 52 position in the helix.

### Inhibitor-binding analysis using ANS as a fluorescence probe

ANS being a strong anion binds predominantly to cationic groups of choline head of DMPC through ion pair

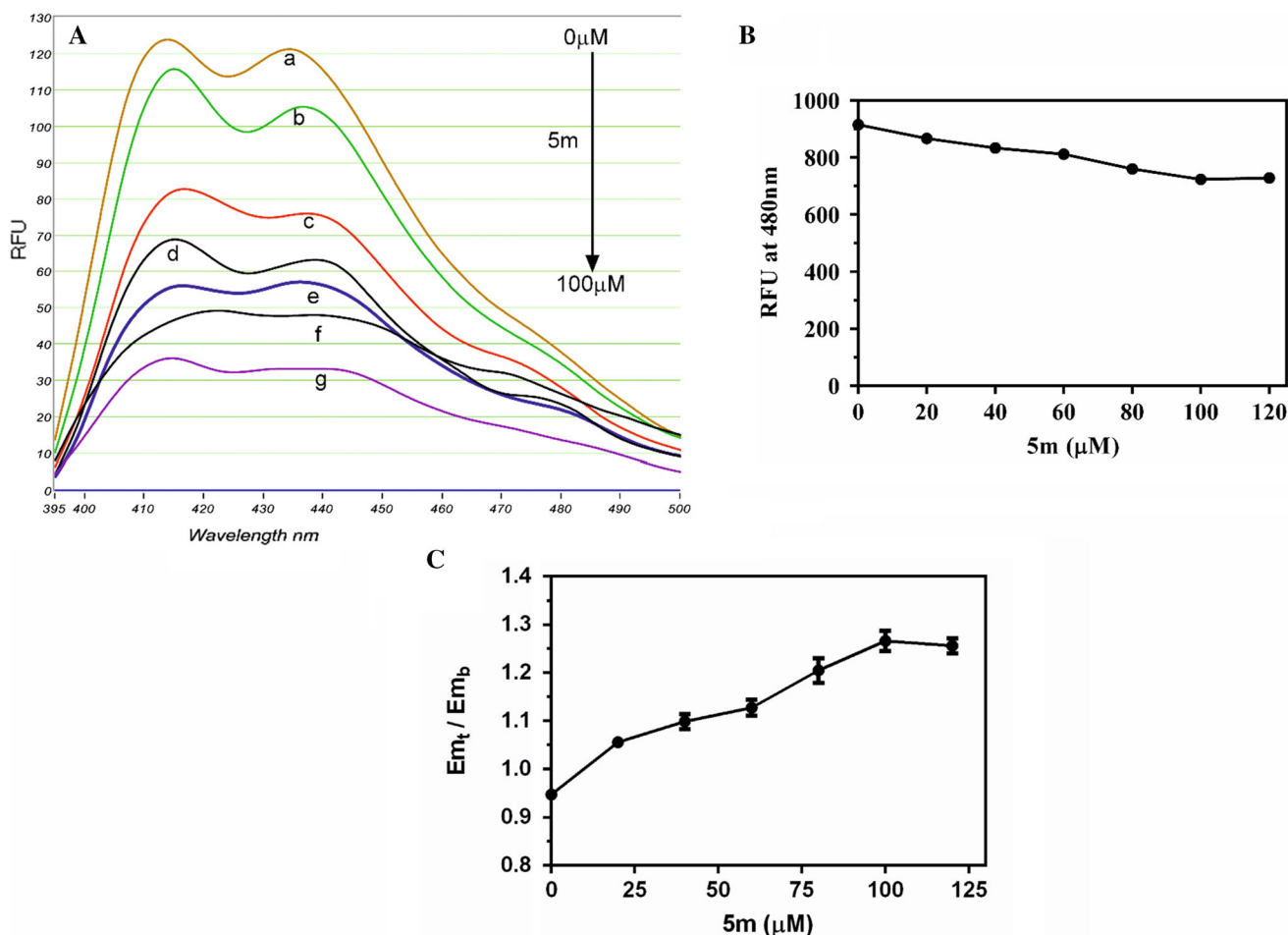
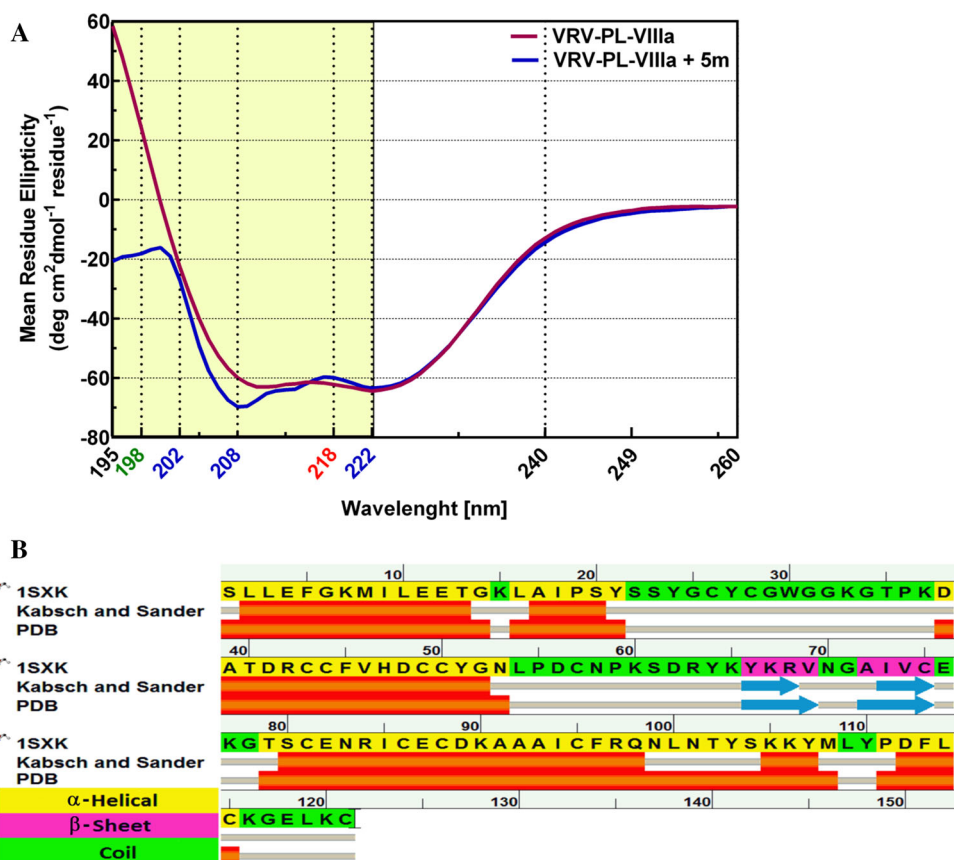


**Fig. 2** **a** Intrinsic fluorescence spectral interaction of VRV-PL-VIIIa with **5m**. Fluorescence spectra were recorded after excitation at 280 nm. Emission intensity was recorded from 395 to 500 nm. Different concentrations of **5m** ranging from 0 to 100 μM, respectively, were recorded. **b** Effect of fluorescence intensity of ANS-DMPC in the presence of **5m**. Emission intensity was recorded at

480 nm. All data values represent mean  $\pm$  SEM ( $n = 6$ ). **c** Inhibitor-binding analysis using ANS as a fluorescence probe:  $E_{m_t}/E_{m_b}$ , where  $E_{m_t}$  and  $E_{m_b}$  are the ECs of ANS in the ternary (DMPC-**5m**-ANS) and in the binary (DMPC-ANS) complexes, respectively. All data values represent mean  $\pm$  SEM ( $n = 6$ )

**Fig. 3 a** Effect of **5m** on secondary structure of VRV-PL-VIIIa. Analysis of far UV-CD spectra for VRV-PL-VIIIa in association with 5  $\mu$ M of **5m**. Spectra for the VRV-PL-VIIIa alone or VRV-PL-VIIIa + **5m** are shown. The spectra shown are unsmoothed and corrected only by subtraction of buffer blanks. The scale on the CD spectra was normalized to MRE. **b** PDB Kabsch and Sander's secondary structure prediction of VRV-PL-VIIIa to elucidate accurate bind mode of **5m**



formation, imparting hydrophobicity resulting in an increase in fluorescence [27]. When these interactions are interrupted, fluorescence of ANS-DMPC decreases. As the concentration of **5m** (0–100  $\mu$ M) is increased, the fluorescence of ANS-DMPC adducts decreases marginally and remains constant at 100  $\mu$ M of **5m**. This clearly suggests that **5m** is competing weakly with ANS binding to DMPC, although the nitrogen atoms present in the 1,3,4 oxadiazole ring at the 2nd and 3rd position of **5m** lacks amphiphilicity (Fig. 2b). Thus, it concludes that **5m** compete very weakly with choline-binding space resulting in perturbed substrate-binding site. Results are evidenced as reported earlier [16]. Further, our results show that EC of **5m** (1.05) is comparatively less than chlorphentermine (4.24) [28] which induces drug-induced phospholipidosis.

#### In silico interaction analysis of 5(a–t) against VRV-PL-VIIIa

Molecular docking and molecular dynamics simulations revealed that GII PLA<sub>2</sub> has a defined conserved active site within a hydrophobic channel lined by invariant hydrophobic residues. The active site residues His48, Asp49, Tyr52, and Asp99 are directly connected to the channel [3, 29]. His48 was known to play a major role in

catalysis by forming hydrogen bonding between Asp99 and Asp49 via water molecule as a part of catalytic network. Thermodynamically, His48 contributes 30 kJ/mol to a total catalytic energy of 40 kJ/mol [29, 30]. It is known that any structural perturbations in His48 of N-terminal  $\alpha$ -helix of PLA<sub>2</sub> play an important role in both membrane binding of the enzyme and substrate binding to the catalytic site that reduces the binding affinity of the enzyme–substrate complex [31]. All the ligands showed interaction with Trp31 which is close to the active site residing at random coil. Depletion in  $\alpha$ -helical and random coil clearly suggests that **5m** binds with His48 ( $\alpha$ -helix), which resides near random coil (Fig. 4a, b); thus, this authenticates the CD data with respect to Kabsch and Sander's secondary structure prediction of VRV-PL-VIIIa (Figs. 3b, 4a). Our MD simulation clearly reveals that all the ligands embedded in the substrate-binding pocket completely blocks the access of the substrate, near the catalytic site (data not shown).

#### In situ inhibition of indirect hemolytic activity of VRV-PL-VIIIa by 5(a–t)

In situ indirect hemolytic activity of VRV-PL-VIIIa, in presence of compound **5m** was evaluated using egg yolk

**Fig. 4** In silico analysis of VRV-PL-VIIIa with **5m**. Docking pose of **5m** with VRV-PL-VIIIa showing molecular interaction before molecular dynamic simulation (a). Binding geometry of **5m** (wired model) with hydrophobic core residing at active site of VRV-PL-VIIIa after MD simulations (b)

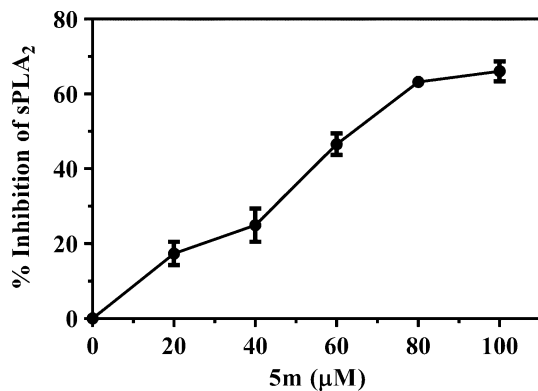
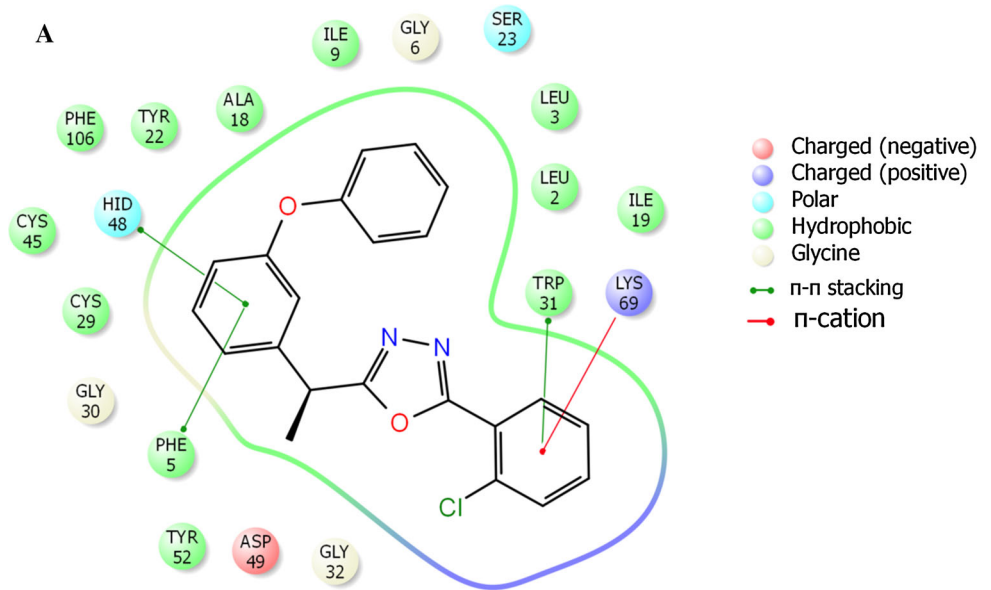


**Fig. 5** Neutralization of indirect hemolytic activity of VRV-PL-VIIIa by **5m**. All data values represent mean  $\pm$  SEM ( $n = 6$ )

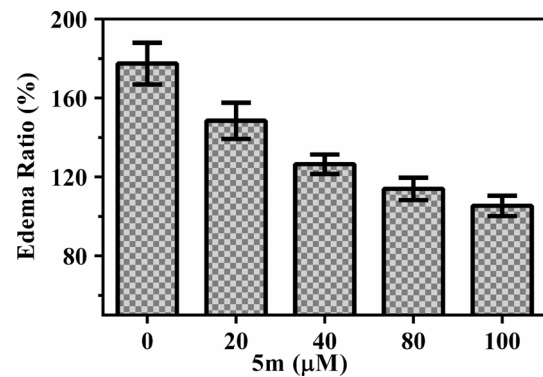


**Fig. 6** Neutralization of edema-inducing activity of VRV-PL-VIIIa by **5m**. All data values represent mean  $\pm$  SEM ( $n = 4$ )

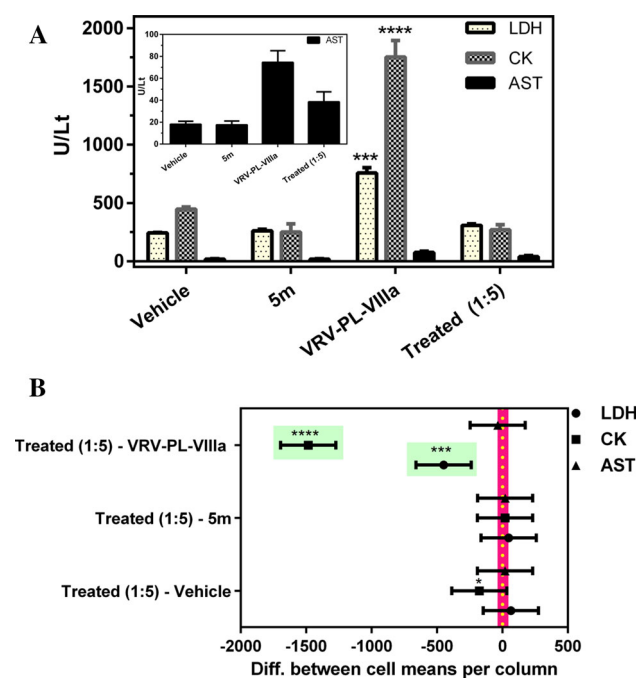


**Fig. 7** Effect of **5m** on serum AST, (*inset*) CK, and LDH activities in mice which received saline (vehicle), VRV-PL-VIIIa (positive control), **5m** (negative control), and treated group VRV-PL-VIIIa + **5m** (1:5, w/w) intramuscular (**a**). Dunnett's test with 99% confidence intervals revealing the band of significance of **5m** with reduced cytosolic and myotoxicity markers when compared to control represented in colored dotted line (**b**). All data values represent mean  $\pm$  SEM ( $n = 4$ ). \* $P < 0.05$ , \*\*\* $P < 0.001$ , \*\*\*\* $P < 0.0001$

and packed erythrocytes as substrate. VRV-PL-VIIIa alone exhibited  $96 \pm 2.0\%$  hemolysis of erythrocyte (positive control) when compared with pure water (100% lysis). VRV-PL-VIIIa incubated with **5m** (0–100  $\mu\text{M}$ ), respectively, for 60 min at 37  $^{\circ}\text{C}$ , inhibited hemolysis in a dose-dependent manner (Fig. 5).

**5m** showed comparatively significant dose-dependent inhibition, induced by VRV-PL-VIIIa compared to positive control.

### In vivo neutralization of edema-inducing activity of VRV-PL-VIIIa by **5m**

The PLA<sub>2</sub> from snake venoms, when injected into the mouse footpad, induced edema in the ratio of more than  $175 \pm 4$  when compared to saline-injected mice. Since sPLA<sub>2</sub>s are edematous in vivo, we examined the effect of **5m** on the edema-inducing activity of VRV-PL-VIIIa at different concentrations ranging from 0 to 100  $\mu\text{M}$ . **5m** inhibited VRV-PL-VIIIa in a concentration-dependent manner (*inset* of Fig. 6). **5m** significantly inhibited edema-inducing activity of VRV-PL-VIIIa (Fig. 6).

### Myotoxicity

VRV-PL-VIIIa is known to possess potent myotoxicity [32]. We evaluated the efficacy of **5m** in neutralizing the myotoxicity of VRV-PL-VIIIa in the ratio of 1:5 (sPLA<sub>2</sub>:**5m**). Intramuscular injection of VRV-PL-VIIIa causes degeneration of muscle fibers resulting in infiltration of polymorphonuclear leukocytes that rupture blood vessels in mice (Fig. 8; M2), when compared to normal healthy controls (Fig. 8; M1) [3, 7]. The mice injected with VRV-PL-VIIIa:**5m** (1:5 w/w) mixture showed decreased levels of CK, LDH, and AST activities (Fig. 7a); this is also associated with decrease in myolysis and infiltration of polymorphonuclear leukocytes in skeletal muscle fibers with intact musculature (Fig. 8; M3) and it is comparable with normal healthy control. 99% of confidence interval (Dunnett's test) shows the band of significance, when compared with the treated group (Fig. 7b).

### Lung hemorrhage

Intraperitoneal injection of VRV-PL-VIIIa is known to induce hemolysis and lung damage resulting in rupture of blood vessels in mice [5, 26]. When a group of mice were injected (i.p.) with half of the LD<sub>50</sub> dose of sPLA<sub>2</sub>, lung damage occurred, which can be visualized by hemolysis and was confirmed by histopathological studies (Fig. 8). Microscopic section of mice injected with saline (control) showed lung parenchyma with normal histology (L1). Positive control mice that received VRV-PL-VIIIa alone, showed lung tissue with areas of interstitial, alveolar hemorrhage associated with intense rupture of blood vessels and intense infiltration of polymorphonuclear leukocytes (L2). The mice injected with sPLA<sub>2</sub> with **5m** (1:5 w/w) showed lung parenchyma with decrease in areas of hemorrhage and rupture of blood vessels with intact red blood cells (L3), which is comparable with normal healthy control.

### Discussion

1,3,4-Oxadiazole is an important class of heterocycles, with a whole array of therapeutic values like analgesic, bactericidal, antifungal, anticonvulsant, psychotropic, plant growth regulating, and mono amino oxidase inhibition. 1,3,4-Oxadiazole exerts dual COX/LOX inhibitors constituting a valuable alternative to classical NSAIDs and selective COX-2 inhibitors for the treatment of inflammatory diseases. But COX and LOX operate downstream inflammatory cascade [15]. So, we attempted to block the upstream main enzyme sPLA<sub>2</sub>, which drives inflammatory

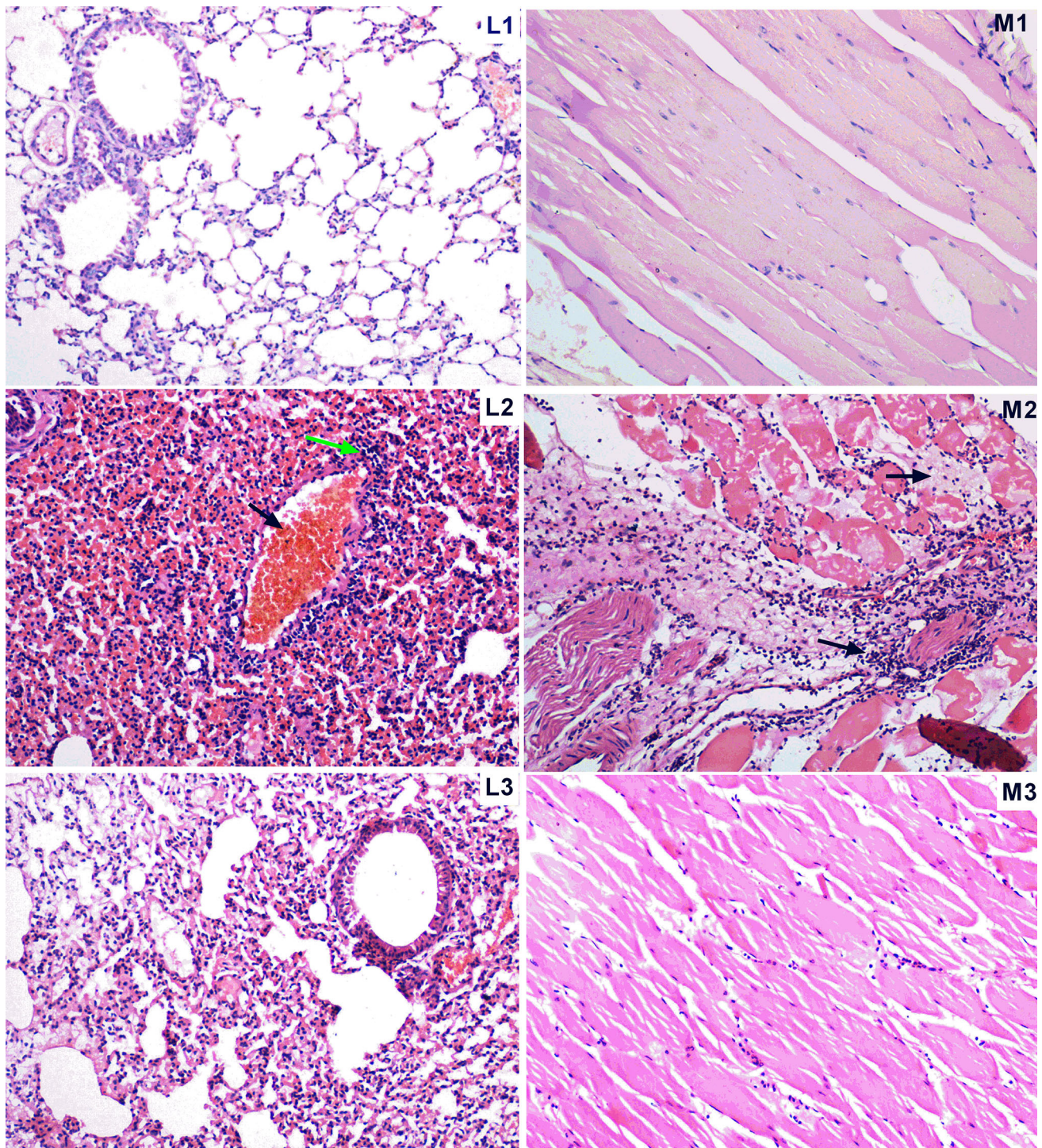


**Fig. 8** Microphotographs ( $H \times E \times 100$ ) of lung and muscle tissue histopathological studies: mice injected (i.m) with saline showed normal skeleton muscle fiber (*M1*) and normal lung parenchyma (*L1*); mice injected with VRV-PL-VIIIa showed skeleton muscle fiber with area of rhabdomyolysis and intense polymorphonuclear infiltrate (*M2*), and lung parenchyma showed extensive interstitial, intense

cascade [33]. Hence, in our study, 2,5-disubstituted-1,3,4-oxadiazoles **5(a-t)** inhibited sPLA<sub>2</sub> in dose-dependent manner with an IC<sub>50</sub> value ranging from 11.52  $\mu\text{M}$  to

polymorphonuclear infiltrate, and alveolar hemorrhage (*L2*); mice injected with VRV-PL-VIIIa-**5m** (1:5, w/w) showed skeleton muscle fiber with decreased polymorphonuclear infiltration (*M3*) and lung showed decreasing interstitial hemorrhage associated with decreased PMN leukocytes (*L3*)

72  $\mu\text{M}$ . Fenopfen was derivatized with 1,3,4 oxadiazole nucleus where chloro/methyl group present at ortho position in case *R* of **5m** to **5p** showed comparative low

**Table 3** Predicted secondary structure percentages of **5m** on VRV-PL-VIIIa

VRV-PL-VIIIa	Native* (%)	% change in presence of <b>5m</b> (treated*)
$\alpha$ -helix	33.3	10.66
$\beta$ -sheet	18.14	3.06
Random coil	48.56	13.72

\* Secondary structure contents were calculated using K2D3 server

effective  $IC_{50}$  value, whereas in case of both ortho and meta position it resulted in higher  $IC_{50}$  (**5n**, **5p**). These results suggest that electronegativity prevailing around the **5m** at ortho (chloro) position binds strongly with the active site of VRV-PL-VIIIa.

However, in case of derivatizing ibuprofen with 1,3,4-oxadiazole nucleus **5(q-t)**, it demanded more electronegativity (**5r**) and hydrophobicity (**5t**) at *R*. These suggest that the orientation of methyl group and chlorine molecule plays an important role in interacting with amino acids at the catalytic site for inhibiting VRV-PL-VIIIa. Noteworthy, these data validate that **5m** is comparatively potent, as

it possesses chlorine at the ortho position and higher hydrophobic moiety at *R*<sub>1</sub> of fenoprofen (Fig. 1). Overall, the result suggested that the change in *R*<sub>1</sub> of **5(a-t)** varies with binding affinity for VRV-PL-VIIIa with substrate. This confirms that the ortho position is most vital for inhibition of sPLA<sub>2</sub> (Table 2). When substrate or ligands bind to active site of the target, it causes conformational change resulting in a change in intrinsic fluorescence [34]. Intrinsic fluorescence spectra of sPLA<sub>2</sub>-**5m** adduct showed quenching of fluorescence in a concentration dependent, suggesting that **5m** interacts with the active site of enzyme (Fig. 2a) as reported earlier [26].

One of the major hypotheses, which explains the strong interaction of inhibitor (amphiphilic amine drugs) with phospholipids, causes inappropriate substrate for phospholipase to act on and thereby results in accumulation of these adducts into lung tissue, which ultimately results in phospholipidosis [28]. Phentermine and chlorphentermine are structurally similar but pharmacologically they differ mainly by two reasons. One is devoid of chlorine and another is phentermine which does not cause phospholipidosis, whereas chlorphentermine causes phospholipidosis, because it contains amphiphilic chlorine molecule.

**Table 4** ADMET evaluation of 2,5-disubstituted 1,3,4-oxadiazole derivatives

Name	Absorption, distribution, metabolism, excretion, and toxicity (ADME/tox)							
	BBB level	HIA level	Solubility level	Hepatotoxicity probability	CYP2D6 probability	PPB level	AlogP98	PSA-2D
<b>5a</b>	1.00	0.00	2.00	0.83	0.77	2.00	4.20	35.08
<b>5b</b>	0.00	0.00	2.00	0.91	0.76	2.00	4.87	35.08
<b>5c</b>	1.00	0.00	2.00	0.74	0.80	2.00	4.03	35.08
<b>5d</b>	1.00	0.00	2.00	0.74	0.80	2.00	4.51	35.08
<b>5e</b>	0.00	0.00	2.00	0.82	0.52	2.00	4.69	35.08
<b>5f</b>	0.00	0.00	1.00	0.93	0.39	2.00	5.36	35.08
<b>5g</b>	1.00	0.00	2.00	0.78	0.52	2.00	4.51	35.08
<b>5h</b>	0.00	0.00	1.00	0.83	0.40	2.00	5.00	35.08
<b>5i</b>	1.00	0.00	2.00	0.81	0.60	2.00	4.03	35.08
<b>5j</b>	1.00	0.00	2.00	0.77	0.73	2.00	4.51	35.08
<b>5k</b>	1.00	0.00	2.00	0.77	0.73	2.00	4.51	35.08
<b>5l</b>	0.00	0.00	1.00	0.74	0.39	1.00	5.00	35.08
<b>5m</b>	<b>0.00</b>	<b>0.00</b>	<b>1.00</b>	<b>0.88</b>	<b>0.71</b>	<b>2.00</b>	<b>5.78</b>	<b>44.01</b>
<b>5n</b>	0.00	1.00	1.00	0.95	0.64	2.00	6.44	44.01
<b>5o</b>	0.00	0.00	1.00	0.89	0.72	2.00	5.60	44.01
<b>5p</b>	0.00	1.00	1.00	0.90	0.67	2.00	6.08	44.01
<b>5q</b>	0.00	1.00	1.00	0.33	0.44	2.00	5.87	35.08
<b>5r</b>	0.00	1.00	1.00	0.49	0.42	2.00	6.53	35.08
<b>5s</b>	0.00	0.00	1.00	0.32	0.49	2.00	5.69	35.08
<b>5t</b>	0.00	1.00	1.00	0.44	0.47	2.00	6.17	35.08
Quercetin (standard)	4.00	1.00	3.00	0.93	0.55	2.00	1.63	130.31

**5m** denotes the potent ligand henceforth it has been highlighted with bold

Hence, **5m** possesses chlorine molecule in its *R* group (Scheme 1). Hence, we have evaluated whether **5m** interacts with choline group in DMPC. Our result showed that **5m** exerts very weak interaction with DMPC (Fig. 2b, c). Hence **5m** does not attribute significant fluorescence intensity of binary (**5m**-DMPC) complex, thereby not triggering drug-induced phospholipidosis, which is a major concern of sPLA<sub>2</sub> inhibitors [28].

Biophysical study indicates that **5m** interacts with sPLA<sub>2</sub> enzyme to bring about inhibition, which is further confirmed by circular dichroism (CD) spectral study. CD data suggest that major secondary changes are substantiated at random coil and  $\alpha$ -helix (Fig. 3a); hence it is evident that **5m** is bringing major changes at active site. Detailed analysis at  $[\theta]\lambda$  ( $\lambda = 198$ ) of VRV-PL-VIIIa + **5m** spectral peak showed a maximum saturation, suggesting a complete abolishment of random coil, whereas at  $[\theta]\lambda$  ( $\lambda = 218$ ) of VRV-PL-VIIIa + **5m** peak a minor change was observed in  $\beta$ -sheet. The change in the percentage of secondary structure of VRV-PL-VIIIa upon interaction with IC<sub>50</sub> concentration of **5m** is summarized (Table 3). To analyze the binding of **5m** with secondary structure of enzyme, active site residues were analyzed by PDB structure and Kabsch–Sander's secondary structure prediction models for VRV-PL-VIIIa using Accelrys discovery (Fig. 3b). The results illustrated that these models are closely related to elucidating  $\alpha$ -helical,  $\beta$ -sheet, and random coils of VRV-PL-VIIIa as reported earlier [26]. These data authenticate that **5m** binds chiefly to random coil and  $\alpha$ -helical of active site. Thus, CD study substantiates the fluorescence data that **5m** interacts closely with enzyme for inhibition. Molecular docking studies showed an interacting map of VRV-PL-VIIIa with compound **5m** (Fig. 4a, b). Based on XP glide score, **5m** showed a promising scoring function, when compared to other structurally related compounds (Table 4). Additionally, the low E model value indicates the best binding affinity between protein and ligand [12]. In general, all the ligands showed interaction with Trp31 which is close to the active site. Importantly, binding of ligands **5m** near the  $\alpha$ -helical random coil clearly suggests that it had interaction with His48, which resides near the random coil. **5m** showed comparatively significant dose-dependent inhibition, induced by VRV-PL-VIIIa compared to positive control. Inhibition of indirect hemolytic activity of VRV-PL-VIIIa was tested with **5m** and found to be more potent when compared to control (Fig. 5).

In vivo toxicological study showed that, VRV-PL-VIIIa affects the vital organs such as the lung, liver, and kidney by causing hemorrhage in victims. Edema inducing activity is an unusual activity of VRV-PL-VIIIa [5, 35, 36]. VRV-PL-VIIIa-induced edema ratio decreased significantly to 50%, when compared to vehicle edematous leg

( $P < 0.0001$ ) (Fig. 6). **5m** inhibited edema-forming activity in a dose-dependent manner. When VRV-PL-VIIIa was injected (i.m) with half of the LD<sub>50</sub> dose, tissue showed bundles of skeletal muscle fibers with areas of myolysis around the injected spot in contrast to the normal healthy control. Microscopic results were confirmed by elevated levels of cytosolic markers such as LDH, AST, and CK activities in case of positive control which received VRV-PL-VIIIa alone [37]. Treated group showed decrease in area of myolysis around the injected spot. VRV-PL-VIIIa induced lung hemorrhage, when injected intraperitoneally to the mice [5]. **5m** showed decrease in areas of interstitial, alveolar hemorrhage associated with intense rupture of blood vessels in VRV-PL-VIIIa-induced group. It was also evident by microscopic observation that infiltration of polymorphonuclear leukocytes was reduced, when compared to the positive control.

## Conclusion

Compounds inhibiting sPLA<sub>2</sub> have been implicated as potential therapeutic agents, in the treatment of inflammatory disorders. Recent studies show that over 50% of patients consuming known NSAIDs like fenoprofen, diclofenac, ibuprofen, undergo major damage in their small intestine [14, 38]. Hence, we targeted the primary enzyme (sPLA<sub>2</sub>), which drives the inflammatory cascade. Results emphasize that 1,3,4-oxadiazole may act as a better pro-drug to block the release of arachidonic acid, which is a substrate for COX-2.

Our experimental data revealed that the structure–activity relationship studies of 1,3,4-oxadiazoles with sPLA<sub>2</sub> correlated with the molecular interaction studies. The binding mode of **5m** involved crucial interactions with important residues for substrate recognition, such as His48 and consequent perturbation of His48 resulted in down-regulation of VRV-PL-VIIIa. **5m** binds within or close to the calcium-binding loop of the catalytic triad, wherein Ca<sup>2+</sup> and His48 reside. Hence, this is validated by ANS–**5m** fluorescent interaction studies, CD and Kabsch–Sander's secondary structure prediction models. Thus, the compound **5m** showed potential anti-inflammatory activity in vitro, in situ, and in vivo studies by targeting sPLA<sub>2</sub>. The present study may lead to developing better inhibitors against venom PLA<sub>2</sub>.

**Acknowledgements** SNS thanks UGC, New Delhi [UGC-MRP Vide No: F. No. 38-220/2009 (SR) dated December 24, 2009]. HKV thanks CSIR, Govt of India for CSIR-Senior Research Fellowship (08/584 (0001)/2012-EMR-I), and TEQIP-II, SJCE for Ph.D. assistantship. We thank Dr. Basappa, Dr. Sharath, Mr. Shankar and IOE, University of Mysore, Mysuru, Schrödinger team, Mr. Govindaraju -MBU (IISC, Bengaluru), Dr. Sunila, and Dr. M. Guruswamy, JSS hospital Mysuru, for their help towards this work.

**Compliance with ethical standards**

**Conflict of interest** The authors have no conflict of interest.

**Appendix**

$$\Delta\text{RFU} = \text{RFU}(\text{control}) - \text{RFU}(\text{test}) \quad (\text{A.1})$$

$$\text{MRE} = \frac{\theta \times (0.1 \times \text{MRW})}{l \times [P]} \quad (\text{B.1})$$

$$\text{MRW} = \frac{M}{N - 1} \quad (\text{B.2})$$

$$\text{Edema ratio}(\%) = \left[ \frac{\text{Edematous limb}}{\text{Normal limb}} \right] \times 100 \quad (\text{C.1})$$

**References**

- Lomonte B, Angulo Y, Calderón L (2003) An overview of lysine-49 phospholipase A<sub>2</sub> myotoxins from crotalid snake venoms and their structural determinants of myotoxic action. *Toxicon* 42:885–901. doi:10.1016/j.toxicon.2003.11.008
- Mohapatra B, Warrell DA, Suraweera W, Bhatia P, Dhingra N, Jotkar RM, Rodriguez PS, Mishra K, Whitaker R, Jha P (2011) Snakebite mortality in India: a nationally representative mortality survey. *PLoS Negl Trop Dis* 5:e1018. doi:10.1371/journal.pntd.0001018
- Kini RM (2003) Excitement ahead: structure, function and mechanism of snake venom phospholipase A<sub>2</sub> enzymes. *Toxicon* 42:827–840
- Iwama S, Matsuda T, Katsumura S, Tani T, Fujii S, Ikeda K, Takehara H (1995) New phospholipase A<sub>2</sub> inhibitor: synthesis and inhibition mechanism of oxazolidinone phospholipid analog. *Bioorg Med Chem* 3:1397–1403
- Kasturi S, Gowda TV (1989) Purification and characterization of a major phospholipase A<sub>2</sub> from Russell's viper (*Vipera russelli*) venom. *Toxicon* 27:229–237. doi:10.1016/0041-0101(89)90136-0
- Jayanthi GP, Veerabasappa Gowda T (1988) Geographical variation in India in the composition and lethal potency of Russell's viper (*Vipera russelli*) venom. *Toxicon* 26:257–264. doi:10.1016/0041-0101(88)90216-4
- Prasad BN, Kemparaju K, Bhatt KGS, Gowda TV (1996) A platelet aggregation inhibitor phospholipase A<sub>2</sub> from Russell's viper (*Vipera russelli*) venom: isolation and characterization. *Toxicon* 34:1173–1185. doi:10.1016/0041-0101(96)00033-5
- Dennis EA (2000) Phospholipase A<sub>2</sub> in eicosanoid generation. *Am J Respir Crit Care Med* 161:S32–S35. doi:10.1164/ajrccm.161.supplement\_1.lta-7
- Dileep KV, Tintu I, Sadasivan C (2011) Molecular docking studies of curcumin analogs with phospholipase A<sub>2</sub>. *Interdiscip Sci Comput Life Sci* 3:189–197. doi:10.1007/s12539-011-0090-9
- Burke JE, Dennis EA (2009) Phospholipase A<sub>2</sub> structure/function, mechanism, and signaling. *J Lipid Res* 50(Suppl):S237–S242. doi:10.1194/jlr.R800033-JLR200
- Wallace JL (1997) Nonsteroidal anti-inflammatory drugs and gastroenteropathy: the second hundred years. *Gastroenterology* 112:1000–1016. doi:10.1053/gast.1997.v112.pm9041264
- Husain A, Ajmal M (2009) Synthesis of novel 1,3,4-oxadiazole derivatives and their biological properties. *Acta Pharm* 59:223–233. doi:10.2478/v10007-009-0011-1
- Jayashankar B, Lokanath Rai KM, Baskaran N, Sh S (2009) Synthesis and pharmacological evaluation of 1,3,4-oxadiazole bearing bis(heterocycle) derivatives as anti-inflammatory and analgesic agents. *Eur J Med Chem* 44:3898–3902. doi:10.1016/j.ejmech.2009.04.006
- Sharma SSP, Kumar N, Dudhe R (2010) A review: oxadiazole their chemistry and pharmacological potentials. *Der Pharm Chem* 2:253–263
- Lowry OH, Rosebrough NJ, Farr AL, Randall RJ (1951) Protein measurement with the folin phenol reagent. *J Biol Chem* 193:265–275
- Vivek HK, Swamy SG, Priya BS, Sethi G, Rangappa KS, Nanjunda Swamy S (2014) A facile assay to monitor secretory phospholipase A<sub>2</sub> using 8-anilino-1-naphthalenesulfonic acid. *Anal Biochem* 461:27–35. doi:10.1016/j.ab.2014.05.024
- Whitmore L, Wallace BA (2008) Protein secondary structure analyses from circular dichroism spectroscopy: methods and reference databases. *Biopolymers* 89:392–400. doi:10.1002/bip.20853
- Louis-Jeune C, Andrade-Navarro MA, Perez-Iratxeta C (2012) Prediction of protein secondary structure from circular dichroism using theoretically derived spectra. *Proteins* 80:374–381. doi:10.1002/prot.23188
- Singh NBS, Kaur P, Sharma S, Singh TP (2004) Crystal structure of a complex formed between phospholipase A<sub>2</sub> and a non-specific anti-inflammatory amino salicylic acid at 1.2 Å resolution. doi:10.2210/pdb1sxk/pdb
- Umme hani RKV, Patar L, Dieudonné M (2014) Molecular dynamics simulation of homology modeled cytosolic Hsp90 isoform from *Arabidopsis thaliana*. *Int J Anal Pharm Biomed Sci* 3:63–80
- Boman HG, Kaletta U (1957) Chromatography of rattlesnake venom; a separation of three phosphodiesterases. *Biochim Biophys Acta* 24:619–631
- Yamakawa M, Nozaki M, Hokama Z (1976) Fractionation of sakhimhabu (*Trimeresurus elegans*) venom and lethal, hemorrhagic and edema-forming activities of the fractions. *Anim Plant Microb Toxins* 1:97–109. doi:10.1007/978-1-4684-0886-7\_10
- Vishwanath B, Kini RM, Gowda TV (1987) Characterization of three edema-inducing phospholipase A<sub>2</sub> enzymes from habu (*Trimeresurus flavoviridis*) venom and their interaction with the alkaloid aristolochic acid. *Toxicon* 25:501–515
- Gutiérrez JMAV, Brenes F, Chaves F (1990) Changes in myofibrillar components after skeletal muscle necrosis induced by a myotoxin isolated from the venom of the snake *Bothrops asper*. *Exp Mol Pathol* 52:25–36
- Misra U, Hitkari A, Saxena AK, Gurtu S, Shanker K (1996) Biologically active indolylmethyl-1,3,4-oxadiazoles, 1,3,4-thiadiazoles, 4H-1,3,4-triazoles and 1,2,4-triazines. *Eur J Med Chem* 31:629–634. doi:10.1016/0223-5234(96)89559-6
- Mohamed R, Shivaprasad HV, Jameel NM, Shekar MA, Vishwanath BS (2011) Neutralization of local toxicity induced by *Vipera russelli* phospholipase A<sub>2</sub> by lipophilic derivative of ascorbic acid. *Curr Top Med Chem* 11:2531–2539
- Jane YC, Ma MJKH, Weber KC (1985) Fluorescence studies of the binding of amphiphilic amines with phospholipids. *J Lipid Res* 26:735–744
- Joshi UM, Rao P, Kodavanti S, Lockard VG, Mehendale HM (1989) Fluorescence studies on binding of amphiphilic drugs to isolated lamellar bodies: relevance to phospholipidosis. *Biochim Biophys Acta* 1004:309–320

29. Ownby CL, de Araujo HSS, White SP, Fletcher JE (1999) Lysine 49 phospholipase A<sub>2</sub> proteins. *Toxicon* 37:411–445. doi:[10.1016/S0041-0101\(98\)00188-3](https://doi.org/10.1016/S0041-0101(98)00188-3)
30. Janssen MJW, van de Wiel WAEC, Beiboer SHW, van Kampen MD, Verheij HM, Slotboom AJ, Egmond MR (1999) Catalytic role of the active site histidine of porcine pancreatic phospholipase A<sub>2</sub> probed by the variants H48Q, H48 N and H48K. *Protein Eng Des Sel* 12:497–503. doi:[10.1093/protein/12.6.497](https://doi.org/10.1093/protein/12.6.497)
31. Yu L, Dennis EA (1991) Critical role of a hydrogen bond in the interaction of phospholipase A<sub>2</sub> with transition-state and substrate analogues. *Proc Natl Acad Sci USA* 88:9325–9329. doi:[10.1073/pnas.88.20.9325](https://doi.org/10.1073/pnas.88.20.9325)
32. Angulo Y, Lomonte B (2009) Biochemistry and toxicology of toxins purified from the venom of the snake *Bothrops asper*. *Toxicon* 54:949–957. doi:[10.1016/j.toxicon.2008.12.014](https://doi.org/10.1016/j.toxicon.2008.12.014)
33. Hosadurga KK, Vivek HK, Hanumantharayappa B, Shobith R, Krishna CB, Lewis HM, Julian EF, Priya BS, Basappa NSS, Andreas B, Rangappa KS (2015) MOLPRINT 2D-based identification and synthesis of novel chromene based small molecules that target PLA<sub>2</sub>: validation through chemo- and bioinformatics approaches†. *RSC Adv* 5:89797–89808. doi:[10.1039/c5ra13085a](https://doi.org/10.1039/c5ra13085a)
34. Jameel NM, Frey BM, Frey FJ, Veerabasappa Gowda T, Vishwanath BS (2005) Inhibition of secretory phospholipase A<sub>2</sub> enzyme by bilirubin: a new role as endogenous anti-inflammatory molecule. *Mol Cell Biochem* 276:219–225
35. Akhter M, Akhter N, Alam MM, Zaman MS, Saha R, Kumar A (2011) Synthesis and biological evaluation of 2,5-disubstituted 1,3,4-oxadiazole derivatives with both COX and LOX inhibitory activity. *J Enzyme Inhib Med Chem* 26:767–776. doi:[10.3109/14756366.2010.550890](https://doi.org/10.3109/14756366.2010.550890)
36. Anilkumar NC, Sundaram MS, Mohan CD, Rangappa S, Bulusu KC, Fuchs JE, Girish KS, Bender A, Rangappa KS (2015) A one pot synthesis of novel bioactive tri-substitute-condensed-imidazopyridines that targets snake venom phospholipase A<sub>2</sub>. *PLoS ONE* 10:e0131896. doi:[10.1371/journal.pone.0131896](https://doi.org/10.1371/journal.pone.0131896)
37. Davy CW, Trennery PN, Edmunds JG, Altman JFB, Eichler DA (1987) Local myotoxicity of ketamine hydrochloride in the marmoset. *Lab Anim* 21:60–67. doi:[10.1258/002367780740725](https://doi.org/10.1258/002367780740725)
38. Higuchi K, Umegaki E, Watanabe T, Yoda Y, Morita E, Murano M, Tokioka S, Arakawa T (2009) Present status and strategy of NSAIDs-induced small bowel injury. *J Gastroenterol* 44:879–888. doi:[10.1007/s00535-009-0102-2](https://doi.org/10.1007/s00535-009-0102-2)